CONF-970783--1 SAND97-1771C

Low-Truncation-Error Finite Difference Equations for Photonics Simulation I. Beam Propagation

G. Ronald Hadley
Sandia National Laboratories*, Albuquerque, New Mexico 87185-5800

ABSTRACT

A methodology is presented that allows the derivation of low-truncation-error finite difference equations for photonics simulation. This methodology is applied to the case of wide-angle beam propagation in two dimensions, resulting in finite difference equations for both TE and TM polarization that are quasi-fourth-order accurate even in the presence of interfaces between dissimilar dielectrics. This accuracy is accomplished without an appreciable increase in numerical overhead and is concretely demonstrated for two test problems having known solutions. These finite difference equations facilitate an approach to the ideal of grid-independent computing and should allow the solution of interesting problems on personal computers.

* Sandia is a multiprogram laboratory operated by Sandia Corporation, a Lockheed Martin Company, for the United States Department of Energy under contract DE-AC04-94AL85000.

I. INTRODUCTION

The design and analysis of photonic circuit elements, both active (diode lasers) and passive (waveguides, switches and couplers) often depends heavily on the science of numerical simulation. Furthermore, this dependence is expected to increase as future optical circuitry becomes more complex and computers more powerful. A large portion of this simulation capability (although by no means all) results from the numerical solution of finite difference equations derived from various simplified forms of the linear Maxwell's Equations. These equations have for the most part been derived by replacing the differential operators in the Maxwell Equations by the standard centered difference operators, resulting in matrix equations that are usually tridiagonal or block-tridiagonal in form. This approach is often denoted by the term "Crank-Nicolson" differencing[1], and results (for uniform grids and materials) in difference equations whose truncation error is quadratic in the spatial grid size. These equations are thus usually referred to as "second-order accurate".

In this and the following paper, we derive finite difference equations of higher accuracy order for photonics simulation applications in one or two space dimensions, and demonstrate their utility on several practical problems of interest. This represents a marked difference from the approach used in the past, where little effort is typically expended in deriving the finite-difference equations, and a maximum of effort in the development of a multitude of numerical techniques for solving the (usually) large matrix equations that result from the practical requirements of reasonable accuracy. Here, we place the emphasis on building as much "intelligence" about the problem as possible into the difference equations, thus allowing the use of coarse grids while still maintaining good solution accuracy. The solution of the resulting

smaller matrix can then be obtained using any of a variety of well-known numerical solution methods. Of course, it stands to reason that more accurate finite difference equations will also allow the solution of larger, more complex problems than have been previously possible. The primary impact of this work is therefore (1) the introduction of a methodology for deriving more accurate finite difference equations whose solutions are considerably less sensitive to the choice of grid employed (an approach to grid-independent computing); and (2) the lowering of the numerical effort required for their solution (especially for higher-dimensional problems) to a level that allows the simulation of interesting problems on a personal computer.

The common second-order procedure referred to above for deriving finite difference equations is widely practiced with only a few exceptions (which shall be pointed out in the text as they occur) primarily because of the complexity of deriving higher-order-accurate equations, an observation certainly confirmed by the derivations reported in this work. However, other arguments sometimes raised against the use of higher-order formulations are found upon closer inspection to be totally without merit. For example, it is often thought that gains in accuracy from higher-order schemes are offset by a loss of stability and numerical robustness. While this may be true for certain nonlinear problems, it does not appear to be true for linear problems, and no such deficiencies have been observed with the several algorithms described here. In addition, there is a common notion that higher-order schemes are more accurate when fine grids are employed, but actually less accurate when used with coarse grids. This argument is also incorrect, due to the presence of still higher-order terms (for example, fifth or sixth order terms in a fourth-order scheme) that become important with coarse grids and cause the steeply-sloping error curve to bend over as the grid becomes coarse. This is an important point, because the greatest advantage of higher-order difference schemes lies in their ability to provide accurate

answers even with *very coarse* grids, resulting in a dramatic savings in runtime for modest problems, and the possibility of solution for otherwise impossible problems. A third misunderstanding is that higher-order schemes increase the bandwidth of the resulting matrix, requiring more sophisticated solution algorithms and slower execution. Contrary to this idea, truncation errors up through fourth order may be achieved routinely with a negligible increase in bandwidth. In fact, all the difference equations described below utilize a stencil of (three)nine points for (1-D)2-D problems, resulting in a bandwidth equal to or just slightly greater than that corresponding to the more common (three)five-point stencil.

In this first paper, we present a precise methodology for deriving finite-difference equations for the important application of 2D wide-angle beam propagation. Our approach is based on Taylor series expansions and includes the field-derivative discontinuities at dielectric interfaces. We then apply this methodology for wide-angle beam propagation, including both TE and TM polarizations, and derive and test the resulting 1-D finite-difference equations using problems with known solutions. The resulting equation is shown to be quasi-fourth-order accurate in the transverse grid size (a designation that will be made precise later on), while retaining the conventional second-order accuracy in the propagation step size. Previous authors[2-6] have attempted to derive higher-order beam propagation algorithms, although these derivations have been deficient in certain respects. Most have been restricted to paraxial propagation and/or a uniform grid. One[5,6] is applicable only for the case of graded-index materials. All have neglected to treat the discontinuities in higher field derivatives at dielectric interfaces, resulting in a lowering of the truncation order at those points. The neglect of these discontinuities limits the accuracy severely for coarse grids.

In the second paper, we derive finite-difference equations for the modeling of the optical fields in a vertical-cavity surface-emitting diode laser (VCSEL). These equations are derived starting from exact finite difference equations describing the eigenmodes of a one-dimensional cavity. The resulting equations for a VCSEL, a device whose character is strongly 1-D-like, thus contain built-in information about the expected solution characteristics and are shown to be highly accurate. An additional advantage of this formalism is that thin material layers (such as quantum wells) can be simulated using grid sizes that differ significantly between adjacent grids without concern about increased truncation error. As in the first paper, the accuracy of this algorithm is tested for problems having known (or approximately known) solutions and compared with that obtained using standard second-order-accurate code.

II. DERIVATION OF FINITE-DIFFERENCE EQUATIONS

We begin with a derivation of the finite-difference equation describing the propagation of a TE- or TM-polarized field through a medium whose refractive index depends only upon one transverse coordinate. Furthermore, we assume that the index is piece-wise constant. The grid is then chosen so that all dielectric boundaries occur at grid points. In this paper the beam propagation algorithm is derived only for longitudinally-uniform structures so that tapers must be modeled using a stair-step procedure. Algorithms designed to include tapered regions *a priori* will be treated in a future publication. Wide-angle beam propagation using the (1,1) Pade approximation is described by the differential equation[7]

$$\left(1+\frac{P}{4k^2}\right)\frac{\partial H}{\partial z}=\frac{iP}{2k}H \tag{1}$$

where $k = \bar{n}k_0$, k_0 is the vacuum wavevector, $\bar{n}$ is the reference index, z is the propagation coordinate, ε is the relative permittivity, and P is the operator

$$P \equiv \frac{\partial^2}{\partial x^2} + k_0^2(\varepsilon - \bar{n}^2)$$

We seek a finite-difference representation of Eq. (1) on the nonuniform grid shown in Fig. 1, where ε takes on the two constant values ε_+ and ε_- as shown. Prerequisite to this, however, are a number of definitions and derivations that must be presented. In particular, a generalization of the first and second derivatives is derived that is valid for a nonuniform grid and includes higher field derivative discontinuities. To develop these prerequisites, we begin by expanding the field in a Taylor series both to the right and left of grid point i:

$$H_{i+1} = H_i + \Delta x_+ H_+^{(i)} + \frac{\Delta x_+^2}{2} H_+^{(ii)} + \frac{\Delta x_+^3}{6} H_+^{(iii)} + \frac{\Delta x_+^4}{24} H_+^{(iv)} + \ldots \tag{2}$$

$$H_{i-1} = H_i - \Delta x_- H_-^{(i)} + \frac{\Delta x_-^2}{2} H_-^{(ii)} - \frac{\Delta x_-^3}{6} H_-^{(iii)} + \frac{\Delta x_-^4}{24} H_-^{(iv)} + \ldots \tag{3}$$

where the superscripts in parentheses denote derivative order and the subscripts on derivatives denote values immediately to the right or left of grid point i. Although almost all quantities in the derivations described here are grid point dependent, we will omit the subscript i in order to simplify notation, leaving the dependence implicit. Forming the linear combination $\varepsilon_+^p \Delta x_-^2 (2) - \varepsilon_-^p \Delta x_+^2 (3)$ (the ε^p factors are inserted for reasons that will soon be evident) and dividing by $\Delta x_+ \Delta x_- (\Delta x_+ + \Delta x_-)$ results in:

$$\begin{aligned} \delta H = {} & \frac{\Delta x_- \varepsilon_+^p H_+^{(i)} + \Delta x_+ \varepsilon_-^p H_-^{(i)}}{\Delta x_+ + \Delta x_-} + \frac{\Delta x_+ \Delta x_-}{2(\Delta x_+ + \Delta x_-)} (\varepsilon_+^p H_+^{(ii)} - \varepsilon_-^p H_-^{(ii)}) + \\ & \frac{\Delta x_+ \Delta x_-}{6} \left(\frac{\Delta x_+ \varepsilon_+^p H_+^{(iii)} + \Delta x_- \varepsilon_-^p H_-^{(iii)}}{\Delta x_+ + \Delta x_-} \right) + \frac{\Delta x_+ \Delta x_-}{24} \left(\frac{\Delta x_+^2 \varepsilon_+^p H_+^{(iv)} - \Delta x_-^2 \varepsilon_-^p H_-^{(iv)}}{\Delta x_+ + \Delta x_-} \right) + \ldots \end{aligned} \tag{4}$$

where

$$p \equiv \begin{cases} 0 & TE \quad Polarization \\ -1 & TM \quad Polarization \end{cases}$$

and

$$\delta H \equiv \frac{\Delta x_- \varepsilon_+^p (H_{i+1} - H_i)}{\Delta x_+ (\Delta x_+ + \Delta x_-)} - \frac{\Delta x_+ \varepsilon_-^p (H_{i-1} - H_i)}{\Delta x_- (\Delta x_+ + \Delta x_-)} \tag{5}$$

is the commonly-used finite-difference approximation to the first derivative for a nonuniform grid, generalized for arbitrary polarization. In a similar manner, the combination $\varepsilon_+^p \Delta x_-(2) + \varepsilon_-^p \Delta x_+(3)$ leads to

$$\delta^2 H = \frac{\varepsilon_+^p H_+^{(i)} - \varepsilon_-^p H_-^{(i)}}{\Delta x_+ + \Delta x_-} + \frac{\Delta x_+ \varepsilon_+^p H_+^{(ii)} + \Delta x_- \varepsilon_-^p H_-^{(ii)}}{\Delta x_+ + \Delta x_-} + \frac{1}{3} \frac{\Delta x_+^2 \varepsilon_+^p H_+^{(iii)} - \Delta x_-^2 \varepsilon_-^p H_-^{(iii)}}{\Delta x_+ + \Delta x_-} + \frac{1}{12} \frac{\Delta x_+^3 \varepsilon_+^p H_+^{(iv)} + \Delta x_-^3 \varepsilon_-^p H_-^{(iv)}}{\Delta x_+ + \Delta x_-} + \ldots \tag{6}$$

where

$$\delta^2 H \equiv \frac{2\varepsilon_+^p (H_{i+1} - H_i)}{\Delta x_+ (\Delta x_+ + \Delta x_-)} + \frac{2\varepsilon_-^p (H_{i-1} - H_i)}{\Delta x_- (\Delta x_+ + \Delta x_-)} \tag{7}$$

is the generalized finite-difference approximation to the second derivative.

From Eqs. (4) and (6) it is apparent that when the derivatives are discontinuous, the commonly-used forms given in Eqs. (5) and (7) correspond to prescribed averages of the first and second derivatives. We thus digress for a moment to concretely define these averages and associated definitions for the purpose of condensing the clumsy notation in Equations (4) and (6). For any (possibly discontinuous) function f, we define the weighted grid average as

$$\langle \Delta x^n f \rangle \equiv \frac{\Delta x_+^{n+1} f_+ + \Delta x_-^{n+1} f_-}{\Delta x_+ + \Delta x_-} \tag{8}$$

and a term proportional to the function discontinuity

$$[f] \equiv \frac{f_+ - f_-}{\Delta x_+ + \Delta x_-} \tag{9}$$

A particularly common form of Eq. (9) is

$$[\Delta x^2] = \Delta x_+ - \Delta x_-$$

the local grid nonuniformity. From Equations (8) and (9) one may easily derive the useful formulas

$$f_\pm = \langle f \rangle \pm \Delta x_\mp [f] \tag{10}$$

$$\langle fg \rangle = \langle f \rangle \langle g \rangle + \gamma [f][g] \tag{11}$$

$$[fg] = [f]\langle g \rangle + \langle f \rangle [g] - [\Delta x^2][f][g] \tag{12}$$

An alternate and sometimes useful form of Eq. (12) is

$$[fg] = [f]\langle g \rangle + \gamma \langle \Delta x^{-2} f \rangle [g] \tag{13}$$

and we have defined

$$\gamma \equiv \Delta x_+ \Delta x_- \tag{14}$$

In terms of the newly-defined symbols, Equations (4) and (6) may be written

$$\langle \varepsilon^p H^{(i)} \rangle = \delta H - \frac{\gamma}{2}[\varepsilon^p H^{(ii)}] - \frac{\gamma}{6}\langle \varepsilon^p H^{(iii)} \rangle - \frac{\gamma}{24}[\Delta x^2 \varepsilon^p H^{(iv)}] - \ldots \tag{15}$$

$$\langle \varepsilon^p H^{(ii)} \rangle = \delta^2 H - \frac{1}{3}[\Delta x^2 \varepsilon^p H^{(iii)}] - \frac{1}{12}\langle \Delta x^2 \varepsilon^p H^{(iv)} \rangle - \frac{1}{60}[\Delta x^4 \varepsilon^p H^{(v)}] - \ldots \tag{16}$$

where we have made use of the polarization-independent interface matching condition

$$[\varepsilon^p H^{(i)}] = 0 \tag{17}$$

Equations (15) and (16) may be further simplified with the use of (11)-(13). In so doing, we drop all terms of order $\Delta x^2(\Delta x_+ - \Delta x_-) + \Delta x^4$ or higher, resulting in a truncation error heretofore referred to as "quasi-fourth-order" (and written as $O(\approx \Delta x^4)$) because it approaches fourth order smoothly in the limit of a uniform grid. All formulas in this work will be truncated to this order. The result is

$$\left\langle \varepsilon^p H^{(i)} \right\rangle = \delta H - \frac{\gamma}{2}\left[\varepsilon^p H^{(ii)}\right] - \frac{\gamma}{6}\left\langle \varepsilon^p H^{(iii)} \right\rangle - \frac{\gamma^2}{24}\left[\varepsilon^p H^{(iv)}\right] + O(\approx \Delta x^4) \tag{18}$$

$$\begin{aligned}\left\langle \varepsilon^p H^{(ii)} \right\rangle = \delta^2 H - \frac{\left[\Delta x^2\right]}{3}\left\langle \varepsilon^p H^{(iii)} \right\rangle - \frac{\gamma_i}{3}\left[\varepsilon^p H_i^{(iii)}\right] - \frac{\left\langle \Delta x^2 \right\rangle}{12}\left\langle \varepsilon^p H^{(iv)} \right\rangle - \frac{\gamma\left[\Delta x^2\right]}{12}\left[\varepsilon^p H^{(iv)}\right] \\ - \frac{\gamma\left\langle \Delta x^2 \right\rangle}{60}\left[\varepsilon^p H^{(v)}\right] + O(\approx \Delta x^4)\end{aligned} \tag{19}$$

Traditionally, the use of a nonuniform grid almost always results in a decrease in truncation order, although this disadvantage is often overshadowed by other advantages such as a reduction in the total number of grid points. For the present formulation, in which all dielectric boundaries are forced to be on grid points, a nonuniform grid is a necessity if a continuum of structural dimensions is to be treated.

Now the quantities in square brackets in Eqs. (18) and (19) (field derivative discontinuities) may be evaluated from the original Helmholtz propagation equation

$$\frac{dH}{dz} - \frac{i}{2k}\frac{d^2H}{dz^2} = \frac{iP}{2k}H \tag{20}$$

from which Eq. (1) is derived as an approximation. If the discontinuity of each term in Eq. (20) is evaluated, the result is

$$[PH] = 0 \tag{21}$$

since the field and its z derivatives cannot be discontinuous. But if we differentiate Eq. (20) with respect to x, multiply by ε^p, and use $\left[\varepsilon^p \frac{\partial H}{\partial x}\right] = 0$, then we get

$$\left[\varepsilon^p \frac{\partial}{\partial x}(PH)\right] = 0 \tag{22}$$

Furthermore, operating on Eq. (20) with P and using Eq. (21) gives

$$\left[P^2 H\right] = 0 \tag{23}$$

and operating in succession first with P and then $\varepsilon^p \frac{\partial}{\partial x}$, together with the use of Eq. (22) results in

$$\left[\varepsilon^p \frac{\partial}{\partial x}(P^2 H)\right] = 0 \tag{24}$$

It may be verified that Equations (21)-(24) are also valid for the Pade propagation Equation (1). Equations (21) and (23) are not useful as they stand. However, simple manipulations using Equations (11) and (12) lead to the useful relations

$$\left[\varepsilon^p PH\right] = \frac{\left[\varepsilon^p\right]}{\left\langle \varepsilon^p \right\rangle}\left\langle \varepsilon^p PH\right\rangle \tag{25}$$

$$\left[\varepsilon^p P^2 H\right] = \frac{\left[\varepsilon^p\right]}{\left\langle \varepsilon^p \right\rangle}\left\langle \varepsilon^p P^2 H\right\rangle \tag{26}$$

The straightforward (but tedious) evaluation of Equations (22),(24),(25) and (26) provides the necessary quantities

$$\gamma\left[\varepsilon^p H^{(ii)}\right] = \eta\left\langle \varepsilon^p H^{(ii)}\right\rangle - \psi\tilde{\varepsilon}_{gm} H \tag{27}$$

$$\gamma\left[\varepsilon^p H^{(iii)}\right] = -\psi\left\langle \varepsilon^p H^{(i)}\right\rangle \tag{28}$$

$$\gamma\left[\varepsilon^{p}H^{(iv)}\right]=\eta\left\langle\varepsilon^{p}H^{(iv)}\right\rangle-\frac{2\psi\tilde{\varepsilon}_{gm}}{\left\langle\varepsilon^{p}\right\rangle}\left\langle\varepsilon^{p}H^{(ii)}\right\rangle-\frac{\psi^{2}\tilde{\varepsilon}_{gm}}{\gamma}\left\{2\eta+\left[\Delta x^{2}\right]\right\}H \tag{29}$$

$$\gamma\left[\varepsilon^{p}H^{(v)}\right]=-2\psi\left\langle\varepsilon^{p}H^{(iii)}\right\rangle-\frac{\psi^{2}\left[\Delta x^{2}\right]}{\gamma}\left\langle\varepsilon^{p}H^{(i)}\right\rangle \tag{30}$$

where we have defined

$$\eta\equiv\frac{\gamma\left[\varepsilon^{p}\right]}{\left\langle\varepsilon^{p}\right\rangle}$$

$$\tilde{\varepsilon}_{gm}\equiv\frac{\varepsilon_{gm}^{2p}}{\left\langle\varepsilon^{p}\right\rangle}=\frac{\left(\varepsilon_{+}\varepsilon_{-}\right)^{p}}{\left\langle\varepsilon^{p}\right\rangle} \tag{31}$$

and

$$\psi\equiv k_{0}^{2}\gamma\left[\varepsilon\right]$$

Inserting Equations (27)-(30) into Equations (18) and (19) results in the following final expressions for the first and second derivatives:

$$\begin{aligned}\left\langle\varepsilon^{p}H^{(i)}\right\rangle=&\left\{1-\frac{\psi\eta}{6}\right\}\delta H-\left\{\frac{\eta}{2}\left(1-\frac{\psi\eta}{6}\right)-\frac{\gamma\psi\tilde{\varepsilon}_{gm}}{12\left\langle\varepsilon^{p}\right\rangle}\right\}\delta^{2}H+\frac{\psi\tilde{\varepsilon}_{gm}}{2}H\\&-\left\{\frac{\gamma}{6}-\frac{\eta\left[\Delta x^{2}\right]}{6}\right\}\left\langle\varepsilon^{p}H^{(iii)}\right\rangle-\frac{\eta}{24}\left\{\gamma-\left\langle\Delta x^{2}\right\rangle\right\}\left\langle\varepsilon^{p}H^{(iv)}\right\rangle\end{aligned} \tag{32}$$

$$\begin{aligned}\left\langle\varepsilon^{p}H^{(ii)}\right\rangle=&\left\{1-\frac{\psi}{6}\left(\eta-\frac{\left[\Delta x^{2}\right]\tilde{\varepsilon}_{gm}}{\left\langle\varepsilon^{p}\right\rangle}\right)\right\}\delta^{2}H+\frac{\psi^{2}\tilde{\varepsilon}_{gm}}{6}\left(1+\frac{\left[\Delta x^{2}\right]}{2\gamma}\left(2\eta+\left[\Delta x^{2}\right]\right)\right)H\\&+\frac{\psi}{3}\left\{1-\frac{\psi\eta}{6}\right\}\delta H-\left\{\frac{\left[\Delta x^{2}\right]}{3}+\frac{\psi}{6}\left(\frac{\gamma}{3}-\frac{\left\langle\Delta x^{2}\right\rangle}{5}\right)\right\}\left\langle\varepsilon^{p}H^{(iii)}\right\rangle\\&-\left\{\frac{\left\langle\Delta x^{2}\right\rangle}{12}+\frac{\eta\left[\Delta x^{2}\right]}{12}\right\}\left\langle\varepsilon^{p}H^{(iv)}\right\rangle\end{aligned} \tag{33}$$

At this point some observations may be made from the form of Equations (32) and (33). First, the typical "centered difference" expressions obtained by using only the terms

δH and $\delta^2 H$ in Equations (32) and (33) result in propagation schemes that are first-order (second-order) accurate between dielectric boundaries for nonuniform (uniform) grids, and first-order accurate even for uniform grids at dielectric boundaries. An improvement in accuracy back to second order may be obtained for uniform grids by simply keeping the first-order interface terms in the above equations. The resulting equations are denoted "improved Crank-Nicolson" in this work and are shown in the test problems below to afford substantial improvements for coarse grids. Second, an improvement in the accuracy beyond second order cannot be obtained by simply keeping more terms in (18) and (19) because the next lowest-order terms involve third derivatives, which cannot be differenced using only a three-point stencil. However, it turns out that if the second derivative is first premultiplied by an appropriate differential operator and then averaged, the resulting expression *can* be accurately represented by a three-point finite difference expression. This procedure depends upon the coefficients in the operator being chosen in such a way that the terms proportional to $\langle \varepsilon^p H^{(iii)} \rangle$ and $\langle \varepsilon^p H^{(iv)} \rangle$ cancel. In particular, following this approach results in the useful quasi-fourth-order expression:

$$\left\langle \varepsilon^p \left(1 + a\frac{\partial}{\partial x} + b\frac{\partial^2}{\partial x^2}\right) H^{(ii)} \right\rangle = \left(1 - \frac{\psi\eta}{6} + \frac{\psi\left[\Delta x^2\right]\tilde{\varepsilon}_{gm}}{6\langle \varepsilon^p \rangle}\right)\delta^2 H + \frac{\psi}{3}\left\{1 - \frac{\psi\eta}{6}\right\}\delta H + \frac{\psi^2 \tilde{\varepsilon}_{gm}}{6}\left\{1 + \frac{\left[\Delta x^2\right]}{2\gamma}\left(2\eta + \left[\Delta x^2\right]\right)\right\} H \tag{34}$$

provided a and b are chosen to be

$$a = \frac{\left[\Delta x^2\right]}{3} + \frac{\psi}{6}\left(\frac{\gamma}{3} - \frac{\langle \Delta x^2 \rangle}{5}\right)$$
$$b = \frac{\langle \Delta x^2 \rangle}{12} + \frac{\eta\left[\Delta x^2\right]}{12} \tag{35}$$

For grid points not on a dielectric boundary, Eq. (34) is equivalent to the simple form

$$\frac{\partial^2 H}{\partial x^2} = \frac{\delta^2 H}{1 + \frac{\left[\Delta x^2\right]}{3}\delta H + \frac{\left\langle \Delta x^2 \right\rangle}{12}\delta^2 H} \tag{36}$$

Equation (36) is the generalization of the well-known Douglas formula[6,8] for the case of a nonuniform grid.

We have now developed the necessary tools to derive the finite-difference approximation to the propagation equation (1). We begin by differencing Eq. (1) with respect to the propagation coordinate z in a centered fashion, yielding second-order accuracy in Δz. (We note in passing that although higher-order differencing methods in the propagation coordinate are derivable, their usefulness is limited by the necessity of keeping the propagation step size small for structures that are z-dependent.) Applying the product of ε^p and the differential operator above to Eq. (1), using (32)-(34), and dropping terms below quasi-fourth order results in the final equation

$$\begin{aligned}
&\left(1+\xi k_0^2\left(\langle\varepsilon\rangle-\bar{n}^2\right)\right)\left\{\left(\left\langle\varepsilon^p\right\rangle+\frac{a\psi\tilde{\varepsilon}_{gm}}{2}\right)H^{n+1}+\left(a+\frac{b\psi}{3}\right)\delta H^{n+1}+\left(b-\frac{a\eta}{2}\right)\delta^2 H^{n+1}\right\} \\
&+\xi\left\{\left(1-\frac{\psi\eta}{6\gamma}\left(\gamma-6b\right)+\frac{\psi\left[\Delta x^2\right]\tilde{\varepsilon}_{gm}}{6\left\langle\varepsilon^p\right\rangle}\right)\delta^2 H^{n+1}+\frac{\psi}{3}\left(1-\frac{\psi\eta}{12}\right)\delta H^{n+1}\right. \\
&\left.+\left(\psi^2\tilde{\varepsilon}_{gm}\left(\frac{1}{12}+\frac{\eta\left[\Delta x^2\right]}{12\gamma}\right)+\psi\left[\varepsilon^p\right]\right)H^{n+1}\right\} = \quad \textit{same with } \xi\to\xi^*,\ H^{n+1}\to H^n
\end{aligned} \tag{37}$$

where the values of a and b are as given in Eq. (35), the superscripts on the field refer to the propagation plane, and we have defined

$$\xi \equiv \frac{1}{4k^2} - \frac{i\Delta z}{4k} \tag{38}$$

Note that the resulting difference Equation (37) is accurate to quasi-fourth order, even on dielectric boundaries. A concern might arise as to whether the added complexity of this equation

and the associated coding might slow execution to a degree sufficient to offset the advantage incurred by the greater accuracy. That this is not the case may be understood by remembering that most of the terms in Eq. (37) drop out for grid points not on a dielectric boundary (which is usually the *vast* majority of the points). In the author's experience, a simple test inserted in the code to identify boundary points typically results in execution times just slightly greater (about 10%) than those observed for second-order-accurate code.

III. ACCURACY COMPARISONS

Here we demonstrate the accuracy of the algorithm just derived by comparing the numerical results obtained on several grids of varying resolution with known answers for two simple test problems. The first involves the computation of the modal index for the fundamental mode of a simple symmetric waveguide. This computation was performed using both the quasi-fourth-order method derived above and also the standard and modified Crank-Nicolson methods. This simple problem was chosen for comparison rather than a more complex problem such as a tilted waveguide[5] because (1) the propagation constant may be computed using other methods to very high accuracy and (2) the modeling of slanted boundaries is considered to be a separate problem requiring additional considerations beyond that of propagation accuracy. Dirichlet boundary conditions with appropriate absorbing regions near the boundaries were also used instead of transparent boundary conditions[9,10] in order to provide more exact accuracy comparisons. However, the algorithm derived above is entirely compatible with transparent boundary conditions, as will be seen in the second test problem. The test problem geometry is detailed in Figure 2. For each algorithm, a trial wave for each polarization was propagated until a

steady state value was obtained and its modal index computed numerically (using a simple intensity-weighted formula). The resulting relative errors in the normalized modal index

$$\tilde{n} \equiv \frac{n - \sqrt{\varepsilon_0}}{\sqrt{\varepsilon_1} - \sqrt{\varepsilon_0}} \tag{41}$$

are Tabulated in Table 1, and plotted versus grid size in Figure 3. Relative errors were calculated based upon normalized modal index values of 0.57451606612441(0.57354315948471) obtained for TE (TM) polarization using a slab waveguide solver. As expected, the standard Crank-Nicolson method leads to errors that depend quadratically on the grid size. The curve denoted "Modified CN TE" is a Crank-Nicolson equation with first-order interface terms from Eqs. (37) and (38) included. Ordinates for the TM case are identical to the TE case and are consequently omitted from the plot. These results are considerably better than the standard Crank-Nicolson case for coarse grids where interface points make up a larger fraction of the total number of grid points. As expected, results obtained using the present method show a fourth-order dependence on grid size (since the grid is uniform) and demonstrate the present formulation to be quite accurate even for very coarse grids. Apparent departures from fourth-order behavior at the finest grid level for the case of TE polarization are probably due to round-off error, since changes in the modal index are occurring in the 13^{th} significant figure and the calculations are performed using double precision arithmetic, with expected uncertainties in the 14^{th} digit.

To emphasize the excellent performance of this algorithm using coarse grids, Figure 4 shows the intensity profile for the converged TE mode on the coarsest grid, constructed by simply connecting intensity values at neighboring grid points with straight lines. It is remarkable that a grid too coarse to smoothly resolve the intensity profile could still result in a reduced

modal index accurate in the third decimal place. Of course, a smoother intensity profile could be constructed on this grid by utilizing information about the higher derivatives.

The second test problem considered is of perhaps greater practical interest, involving the energy exchange between two evanescently-coupled waveguides. The problem geometry is shown in Fig. 5 where once again a uniform grid is employed for maximum accuracy. For convenience, transparent boundary conditions are used at both boundaries[9,10]. The fundamental mode of the left waveguide alone (identical to the waveguide of the previous test) is used as input to the problem, and the distance required for a complete transfer of energy to the rightmost guide and back again is computed. The results are plotted in Fig. 6 versus total number of grid points for both the present algorithm as well as the standard Crank-Nicolson equation (without interface correction terms). Also shown in the figure are approximate lengths (6174.3 μm for TE, 6154.1 μm for TM) obtained from the difference of the propagation constants of the odd and even eigenmodes of the coupled guides as computed from a slab waveguide solver. The latter values must be considered approximate since the mode of the leftmost guide is only an exact combination of the odd and even coupled modes *in the limit of infinite guide separation*. Again the accuracy of the present quasi-fourth-order algorithm for coarse grids is aptly demonstrated compared with the second-order method, which deviates sharply from the correct answer as the grid coarsens.

It should be noted that the algorithm described in this work is non-unitary and therefore does not conserve the intensity integral exactly. This condition results from both the inclusion of the interface terms and also the use of a non-uniform grid. Generally speaking, the deviation from exact conservation increases as (1) the index contrast at a dielectric interface (experiencing

significant field intensity) increases, and (2) the difference between adjacent grid sizes increases. However, no instability has been observed so far, but rather only cyclical variations in beam energy. Usually these are small in magnitude for reasonable grids, and because they are cyclical, do not appear to degrade the accuracy of energy-loss calculations over long propagation distances. (Some of the eigenmode calculations described above were run for distances of 150 mm or more without experiencing a significant overall energy loss).

CONCLUSION

In summary, we have presented a new methodology for the derivation of highly-accurate finite-difference equations for beam propagation. This methodology was used to derive a 2D propagation equation in cartesian coordinates for both TE and TM polarizations. The resulting equation is quasi-fourth-order accurate, but nonetheless still tridiagonal in form and thus solvable using the standard Thomas algorithm. Accuracy tests for both a single waveguide and coupled waveguides confirm the predicted accuracy and demonstrate the utility of these equations even for very coarse grids. The primary impact of this work is twofold: first, the application of the formalism developed here to photonics simulation results in code that is relatively insensitive to the choice of grid (grid-independent computing). This implies that the solution of interesting problems on any reasonable grid will provide answers of sufficient accuracy for design purposes. It therefore frees the researcher (who may not be familiar with numerical computation issues) from concerns about truncation errors and the necessity of running the problem on a number of different grids to be certain that they are not influencing the answer. Second, the resulting coarser grids should reduce runtimes sufficiently so that modest problems can be solved on personal computers and large previously-intractable problems on workstations. These improvements are

expected to be particularly impressive when the approach detailed here is extended to higher-dimensional problems where the numerical effort is considerably more sensitive to the grid resolution. Such an extension to beam propagation problems involving two transverse dimensions is straightforward (but tedious) except for corner points (which are known to be particularly troublesome[11]) and will be described in detail in a future publication.

REFERENCES

1. R. D. Richtmeyer and K. W. Morton, Difference Methods for Initial Value Problems, Second Edition, Interscience Publishers, J. Wiley and Sons, New York, New York.

2. D. Yevick, B. Hermansson, and M. Glasner, "Fresnel and Wide-Angle Equation Analyses of Microlenses", IEEE Photonics Tech. Lett. 2, pp.412-414(1990).

3. L. Sun and G. L. Yip, "A modified finite difference beam propagation method using the Douglas scheme", Optics Lett. 18, pp.1229-1231(1993).

4. R. Pregla, "Higher order approximation for the difference operators in the method of lines", IEEE Microwave and Guided Wave Letters, vol 5, No. 2, pp.53-55(1995).

5. J. Yamauchi, J. Shibayama, and H. Nakano, "Wide-angle propagating beam analysis based on the generalized Douglas scheme for variable coefficients", Optics Lett. 20, pp 7-9(1995).

6. J. Yamauchi, J. Shibayama, M. Sekiguchi, H. Nakano, "Finite-Difference Beam Propagation Method Based on the Generalized Douglas Scheme for a Non-Uniform Grid", IEEE Phot. Tech. Lett. Vol. 9, No. 1 pp67-69(1997).

7. G. R. Hadley, "Wide-angle beam propagation using Pade approximant operators", Optics Lett. 17, pp 1426-1428(1992).

8. A. R. Mitchell, Computational Methods in Partial Differential Equations, John Wiley and Sons, Ltd. 1969, Chap. 2.

9. G. R. Hadley, "Transparent boundary condition for beam propagation", Optics Lett. 16, pp 624-626(1991).

10. G. R. Hadley, "Transparent Boundary Condition for the Beam Propagation Method", IEEE Journal of Quantum Elect. QE-28, pp363-370(1992).

11. A. S. Sudbo, "Why Are Accurate Computations of Mode Fields in Rectangular Dielectric Waveguides Difficult?", J. Lightwave Tech. 10, pp 418-419(1992).

Table 1

Polarization	TM			TE		
N\Method	Standard	Modified	Present	Standard	Modified	Present

Polarization	TM			TE		
	CN	CN	Work	CN	CN	Work
1	0.5371676 0.0640	0.5768063 5.69×10^{-3}	0.57390475 6.30×10^{-4}	0.5377357 0.0640	0.5777236 5.58×10^{-3}	0.5748749 6.25×10^{-4}
2	0.5640013 0.0166	0.5775562 7.00×10^{-3}	0.57356158 3.21×10^{-5}	0.5647636 0.017	0.5785115 6.95×10^{-3}	0.57453422 3.16×10^{-5}
4	0.5711639 4.15×10^{-3}	0.5749984 2.54×10^{-3}	0.57354422 1.84×10^{-6}	0.5720324 4.32×10^{-3}	0.5759671 2.52×10^{-3}	0.574517105 1.81×10^{-6}
8	0.5729721 9.96×10^{-4}	0.5739658 7.37×10^{-4}	0.573543224 1.12×10^{-7}	0.5738919 1.09×10^{-3}	0.5749375 7.33×10^{-4}	0.5745161293 1.10×10^{-7}
16	0.5734134 2.26×10^{-4}	0.5736563 1.97×10^{-4}	0.57354316353 7.05×10^{-9}	0.5743599 2.72×10^{-4}	0.5746289 1.96×10^{-4}	0.57451607000 6.75×10^{-9}
32	0.57351732 4.51×10^{-5}	0.57357238 5.09×10^{-5}	0.57354315975 4.64×10^{-10}	0.57447701 6.80×10^{-5}	0.57454521 5.07×10^{-5}	0.574516066591 8.12×10^{-10}

Table 2

Polarization	TM		TE	
N\Method	Standard CN	Present Work	Standard CN	Present Work
1	5869	6167	5884	6187.5
2	6086.5	6164	6103.5	6182
4	6142	6163	6162.5	6182
8	6158	6163	6178.5	6183.5

TABLE CAPTIONS

1. Normalized modal index for the waveguide described in Fig. 2 computed using various propagation schemes and grids. Just below the modal index is the relative error based on a correct value of 0.5745160661244(0.5735431594847) for TE(TM) modes obtained from a slab waveguide solver. The parameter N in the leftmost column labels the uniform grids as detailed in Fig. 2.

2. Predicted propagation length for energy transfer into the second guide and back again for the geometry shown in Fig. 5. The values may be compared with approximate analytic results (shown as horizontal lines) of 6174.3μm(6154.1μm) for TE(TM) modes. The parameter N in the leftmost column labels the uniform grids as detailed in Fig. 5.

FIGURE CAPTIONS

1. Schematic diagram showing the nomenclature and convention used in the derivation of the finite-difference propagation equation. All dielectric interfaces are assumed to lie on a grid point as shown in the figure.

2. Schematic diagram of waveguide and grid geometry used for propagation constant test. Dielectric constants are $\varepsilon_0 = (11.044,0.)$,$\varepsilon_1 = (11.088,0.)$, $\varepsilon_2 = (11.044,0.004)$. Other parameters are as shown, and the number of grid points in each region are scaled by the integer N.

3. Relative accuracy of computed propagation constant for structure shown in Fig. 1 using various propagation methods. Curve for Modified CN and TM polarization was virtually identical to the TE case and was omitted from the plot.

4. Intensity profile for the converged TE solution to the simple waveguide problem described in Fig. 1 using the coarsest grid. The vertical lines mark the waveguide position. In

order to emphasize the coarseness of the grid, no attempt was made to utilize a computed knowledge of higher-order derivatives and thus smooth the profile.

5. Schematic diagram of waveguide structure for coupling test. Dielectric constants and grid scaling are the same as listed in Fig. 1.

6. Computed length for energy transfer to second waveguide and back again for various grids using both the standard Crank-Nicolson and quasi-fourth-order methods. Approximate answers of 6174.3 μm(6154.1μm) for TE(TM) polarization determined from the difference of the odd and even coupled waveguide eigenmodes is shown as the horizontal dotted lines.

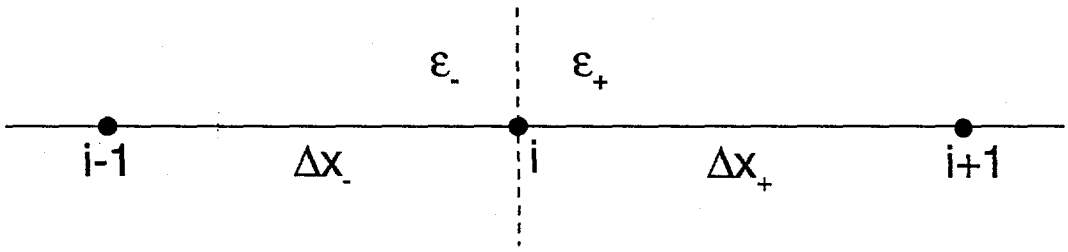

Fig 1

λ_0=1.0μm

n_{ref}=3.327

Δz=0.1μm

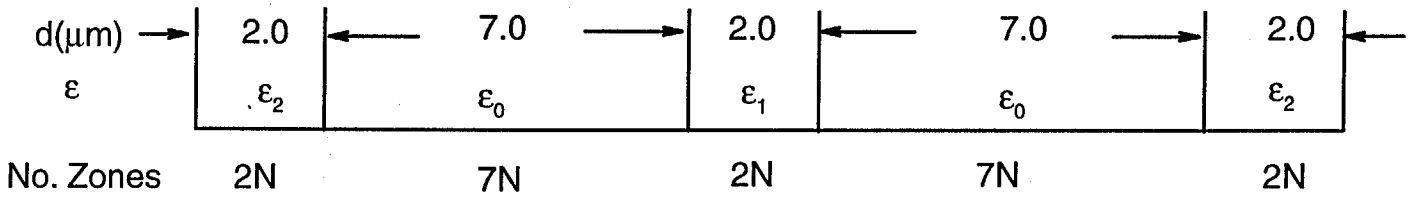

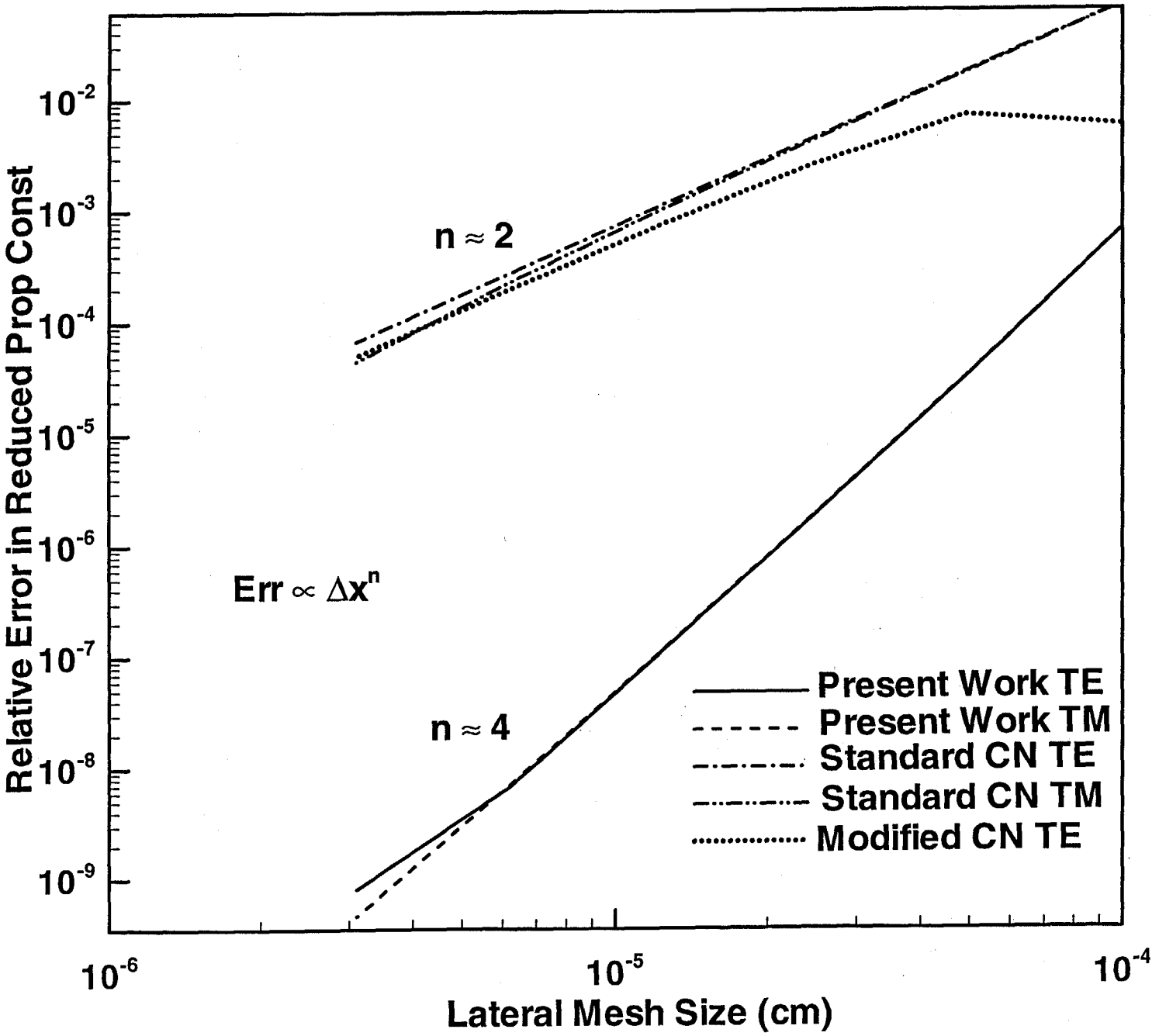
Relative Error in Reduced Prop Const
10^{-2}
10^{-3}
10^{-4}
10^{-5}
10^{-6}
10^{-7}
10^{-8}
10^{-9}
n ≈ 2
Err ∝ Δx^n
n ≈ 4
Present Work TE
Present Work TM
Standard CN TE
Standard CN TM
Modified CN TE
10^{-6}
10^{-5}
10^{-4}
Lateral Mesh Size (cm)

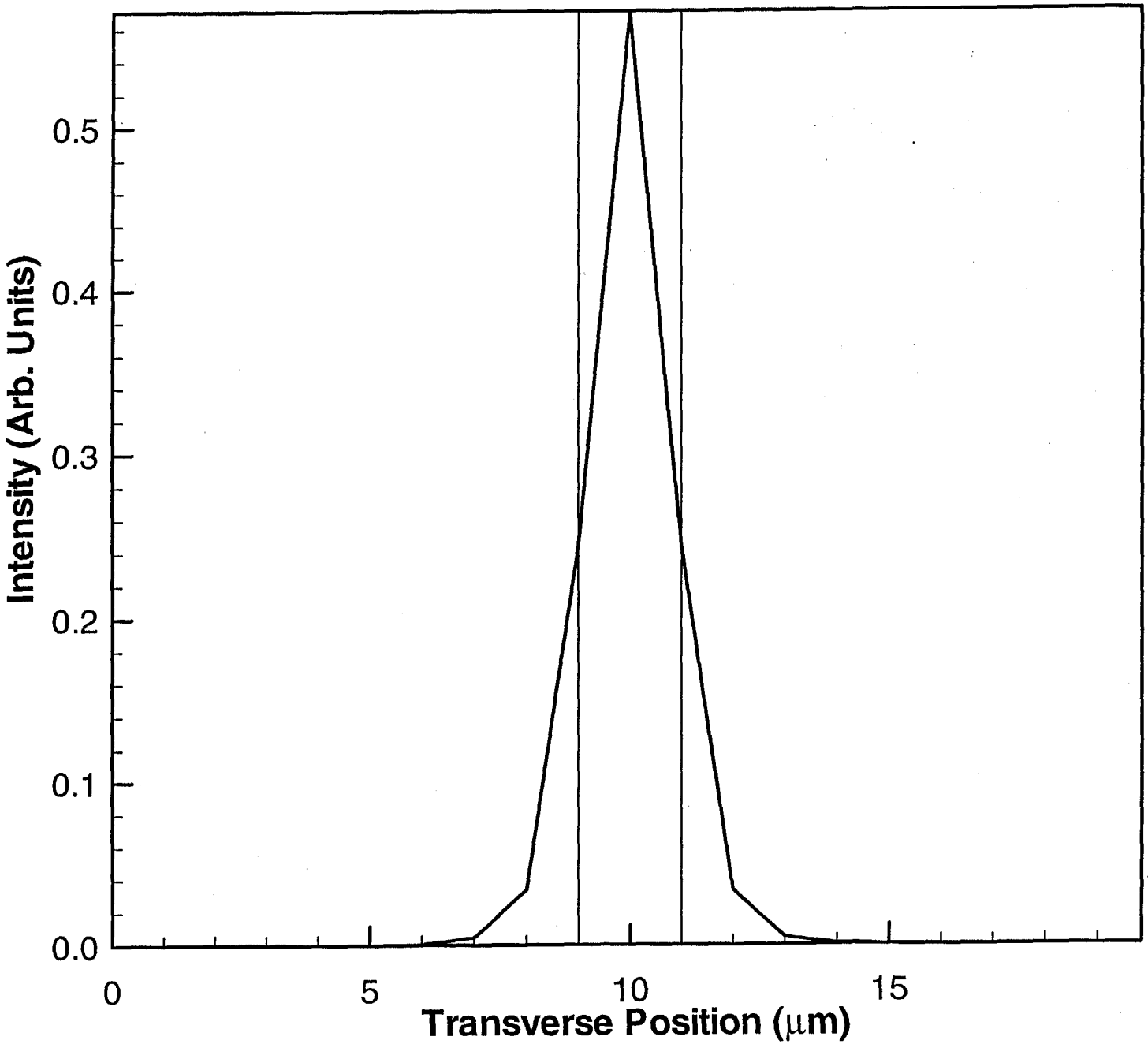
Intensity (Arb. Units)
0.0
0.1
0.2
0.3
0.4
0.5
0
5
10
15
Transverse Position (μm)

Fig 4

λ_0=1.0μm

n_{ref}=3.327

Δz=0.1μm

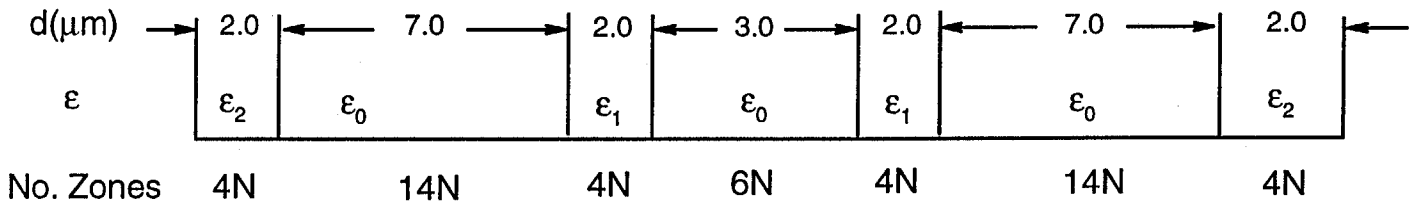

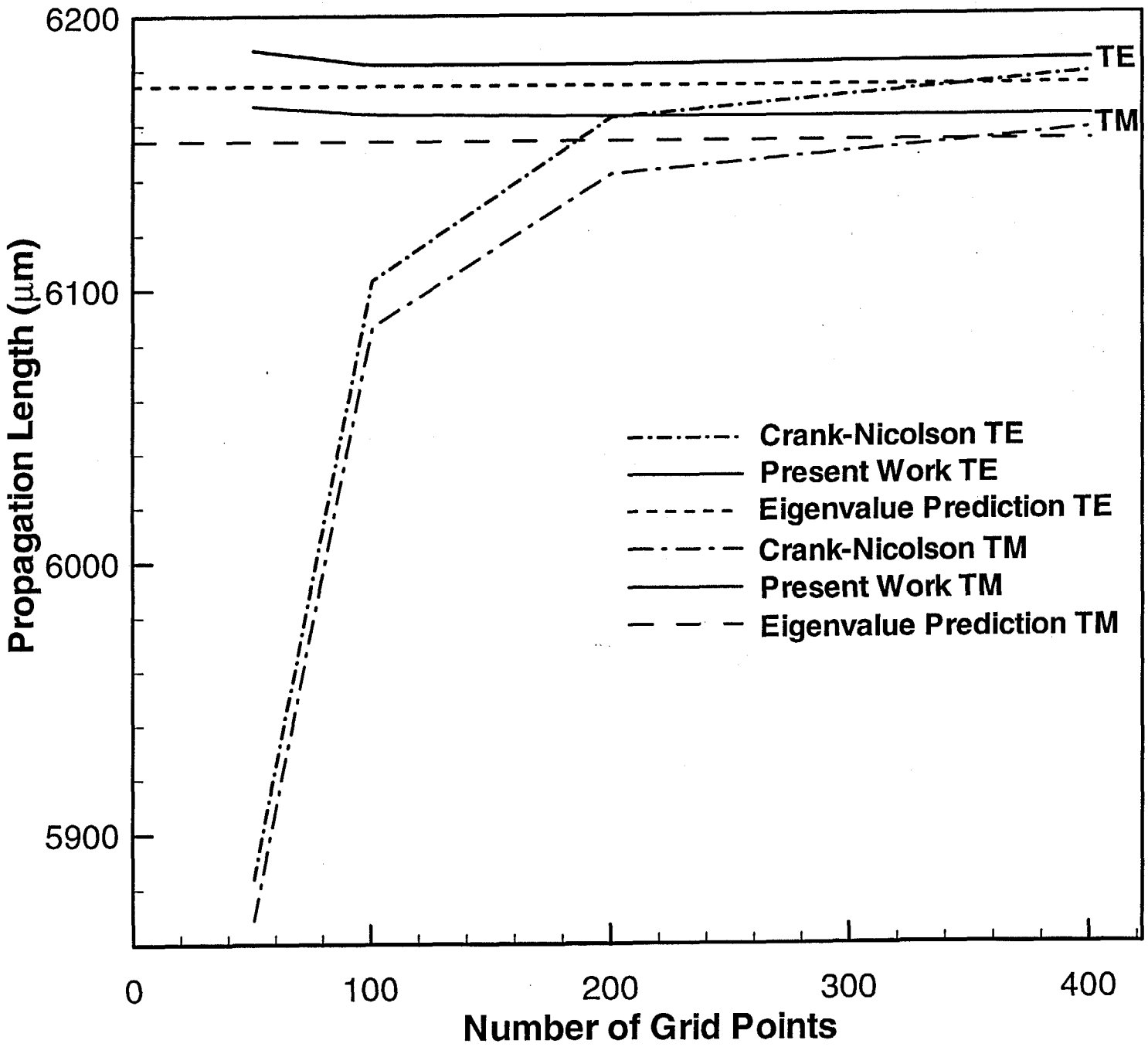
6200
6100
6000
5900
Propagation Length (μm)
0
100
200
300
400
Number of Grid Points
TE
TM
Crank-Nicolson TE
Present Work TE
Eigenvalue Prediction TE
Crank-Nicolson TM
Present Work TM
Eigenvalue Prediction TM